ORNL/TM-8593

ORNL/TM--8593

DE83 005171

Contract No. W-7405-eng-26

Solid State Division

PHYSICAL SPUTTERING OF CANDIDATE PLASMA-SIDE MATERIALS FOR FED/INTOR

J. B. Roberto

Date Published - January 1983

Prepared as input to the U. S. contribution to the
International Tokamak Reactor Phase 2-A Workshop
USA FED-INTOR/82-1, October 1982

Oak Ridge National Laboratory
Oak Ridge, Tennessee 37830
operated by
Union Carbide Corporation
for the
U. S. Department of Energy

CONTENTS

Physical Sputtering of Candidate Plasma-Side Materials for FED/INTOR

J. B. Roberto
Solid State Division
Oak Ridge National Laboratory
Oak Ridge, Tennessee 37830

Abstract

Physical sputtering data are reviewed for a variety of candidate plasma-side materials for fusion reactor applications. Normal incidence sputtering yields are presented for both light and heavy ions (including H, D, ^{4}He, and self-ions) on Be, B, C, SiC, TiC, V, stainless steel, Mo and W targets for energies ranging from the sputtering threshold up to 10 keV and higher. The available data are compared with model calculations for H, D, T, ^{4}He, and self-ion sputtering of the candidate materials. The influence of angle of incidence, surface composition and morphology, and target temperature is discussed. The sputtering of multi-component targets and the energy and angular distributions of sputtered atoms are also considered. It is found that the existing data and models are adequate for factor-of-two estimates of physical sputtering yields for most of the relevant energies and ion-target combinations.

Introduction

Physical sputtering is the energetic removal of a near surface atom from a solid target as a result of an atomic collision sequence initiated by an incident energetic particle. In general, the collision sequence will involve many target atoms and the sputtering process can be described by transport equations (1). For light ions at low energies, an analytic solution is not possible and numerical (2), Monte Carlo (3-4) and empirical (5-6) approaches have been developed to describe the sputtering. A wide variety of sputtering data can be represented using these available formalisms.

In fusion devices, sputtering contributes to impurity introduction and to the erosion and surface modification of plasma-side materials. The sputtering process is extremely sensitive to surface properties since sputtered atoms originate within the first few monolayers of the target surface. This is particularly important in fusion environments where sputtering can occur during the simultaneous release, deposition and diffusion of a wide variety of atomic and molecular species. Sputtering yields can also be significantly modified by related chemical effects such as the formation of oxides and volatile compounds. These phenomena fall in the category of chemical sputtering and are discussed only briefly here.

In this report, physical sputtering data are presented for light ions (H, D, ^{4}He) and self-ions on Be, B, C, SiC, TiC, V, stainless steel, Mo, and W targets. These materials represent a wide range of candidate materials for plasma-side components in FED/INTOR. Energies $\leq$10 keV are considered in detail, and available data at higher energies

are also included. Normal incidence sputtering yields are given and compared with model calculations. The effects of angle of incidence, surface composition and morphology, and temperature are discussed. Angular and energy distributions of sputtered particles and sputtering of multi-component systems are also considered. It is generally found that the existing data for physical sputtering in these materials is adequate when considered in relation to uncertainties in surface conditions and edge temperatures in fusion devices.

Sputtering Models

A general formulation of sputtering has been developed by Sigmund (1) in the form of an analytic solution to linear transport equations. The sputtering yield Y as a function of a normally incident particle at energy E is written

$$Y(E) = \frac{0.042}{E_B N} \alpha (M_2/M_1) S_n (E, Z_1, Z_2) \qquad (1)$$

where E_B (eV) is the surface binding energy (often taken as the sublimation energy), N ($Å^{-3}$) is the target atomic density, and $M_{1,2}$ and $Z_{1,2}$ are projectile and target masses and atomic numbers, respectively. The mass-ratio-dependent function α can be determined experimentally or estimated theoretically and S_n is the nuclear stopping power at the surface. Equation 1 establishes the theoretical basis of the surface binding energy and nuclear stopping power in the general description of sputtering.

For low-energy light ions, the atomic collision sequence leading to sputtering is not sufficiently randomized to justify approximations underlying Equation 1. A numerical solution of the transport equations

is possible and the ANISN code (7) has been adapted for this purpose (2). ANISN calculations are in reasonable agreement with measured sputtering yields for low-energy light ions and reproduce the dependence of the sputtering yield on the angle of incidence (2). The Monte Carlo binary collision codes MARLOWE (3) and TRIM (4) can also be applied to the low-energy light ion regime. MARLOWE allows explicit treatment of target crystallinity. The faster TRIM code is applicable to amorphous targets and is the most widely used sputtering code.

In the threshold region (up to ~10 keV for light ions), empirical relations provide the best estimates of sputtering yields. One such relation (5) is based on the observation that the energy dependence of sputtering yields in this region can be described using an energy parameter $E' = E/E_{th}$ where E_{th} is the threshold energy for sputtering. The total sputtering yield at normal incidence is written

$$Y = Q\,(M_1, M_2, E_B)\; Y_N\,(E') \qquad (2)$$

where Q is a fitting parameter and Y_N is the normalized sputtering yield given by

$$Y_N = 8.5 \times 10^{-3}\; E'^{1/4}\; (1 - \tfrac{1}{E'})^{7/2} \quad . \qquad (3)$$

Simple approximations are available (5) for Q and E_{th} which allow estimates of normal incidence sputtering yields within a factor of two for most materials up to $E' = 20$. For higher energies, Y_N can be modified (5) by the ratio $S_n(E')/S_n(20)$ consistent with Equation 1.

In Figure 1, calculated yields using Equation 2 (with the above modification for $E' > 20$) are compared with normal incidence sputtering

yield data for light and heavy ions on Mo at energies up to 100 keV. The agreement is excellent, although it should be pointed out that Q and E_{th} were experimentally determined for this fit. Experimental data for Q and E_{th} are available for a wide variety of materials (8). We will refer to Equation 2 as the IPP model.

The computer code DSPUT (6) represents another empirical approach to physical sputtering yields. In this model, recent physical sputtering data have been incorporated into an analytical expression for the sputtering yield in terms of $M_{1,2}$, $Z_{1,2}$ and E_B. Angle of incidence effects are also included using an empirical angular-dependent function for light ions below 10 keV. The DSPUT code can be used to calculate normal incidence yields for both light and heavy ions on all targets at energies up to 100 keV. The fit to existing data is not as good as the IPP model (particularly in the threshold region) but the practical application of the code is somewhat simpler. A comparison of DSPUT calculations with experimental data and the IPP model is shown in Figure 1.

Normal Incidence Yields

Normal incidence sputtering yields for the various ion-target combinations considered in this survey are shown in Figures 2-10. Most of the recent and more complete studies through mid-1982 are included. Approximately two-thirds of the presented data are available in two compilations. Anderson and Bay (9) have collected all physical sputtering data for single element targets through mid-1977. Roth, Bohdansky and Ottenberger (8) compiled the

extensive set of low-energy light ion sputtering data from their group in 1979. The data for light ion sputtering are fairly complete for energies up to 10 keV. Self-sputtering data are available for only a limited number of targets and considerable reliance on extrapolations from inert gas sputtering is required. In each figure, the data are compared with estimates from the IPP and DSPUT models. Calculated yields for T ions are also shown. Summary data for D and self-ion sputtering of the candidate materials are presented in Table I.

For Be, the measured yields compare very well with yields for BeO (8) and are probably more representative of the oxide surface. The C data are for room temperature; substantially increased yields are expected at higher temperatures (10-12) due to chemical and other effects. Self-sputtering yields are generally much larger than light ion yields and can lead to catastrophic increases in impurity introduction if they exceed unity. From the data in Table I, normal incidence self-sputtering yields of less than unity are expected at all energies for the lighter targets Be, B, C, and possibly SiC and TiC. Self-sputtering yields exceed unity in V, stainless steel, Mo and W for energies above 0.6 - 1 keV. Self-sputtering yields may also exceed unity for lighter targets at grazing angles of incidence. Qualitative estimates of the accuracy of the data range from ±30% for light ions in stainless steel to factors of 2-4 in some self-ion cases. The data are more reliable near the peaks in the sputtering curves where the yields are larger and less energy-dependent. Physical sputtering in these materials is independent of projectile charge and the sputtered species are primarily (>90%) neutral atoms (5).

Angle of Incidence Effects

Sputtering yields generally increase as incident particle trajectories move away from the surface normal. The effect is most pronounced for light ions above a few keV. Measured total yields (8) for 8 keV H sputtering of Mo at 80 degrees from the surface normal are a factor of twenty greater than normal incidence yields. TRIM calculations (13) indicate maximum enhancements of ~40 times for D sputtering of Ni, Mo and W above 40 keV. Heavy ion yields show maximum increases compared to normal incidence of factors of two near 1 keV (14) and 3-6 at 20-40 keV (9). The maximum in the sputtering yield usually occurs at 60-70 degrees from the surface normal for heavy ions and near 80 degrees for light ions. The yields fall at larger angles due to increased particle reflection at grazing incidence. The available experimental data are summarized in Figure 11.

Within the framework of the Sigmund theory (1), the total sputtering yield should vary as $\cos^{-f}\theta$ where f is between 1 and 2. This result does not adequately represent the range of available data. For heavy ions around 1 keV, the angular-dependent yields follow a simple functional relationship suggested by Oechsner (14). For light ions below 10 keV, Smith et al. (6) have fit the available data with an analytical expression. The computer codes ANISN (7) and TRIM (15) have produced the best agreement with the light ion data and have been used to investigate angular dependent sputtering processes. Calculated angular-dependent yields are compared with experimental results in Figure 11. Additional data can be found in refs. 2, 8, 9, 13 and 14.

Surface Effects

Plasma-side surfaces in fusion devices are exposed to a dynamic deposition and release process often leading to undefined and changing surface conditions. Sputtered particles originate in the first few monolayers of the target, and sputtering yields are extremely sensitive to the composition and binding energy at the surface. Surfaces exposed to significant impurity fluxes (such as limiters and divertor plates) will necessarily accumulate redeposited material since sputtering yields greater than unity cannot be tolerated. All surfaces are possible candidates for hydrocarbon and oxide contamination which can also significantly affect sputtering yields. Surface conditions probably represent the largest uncertainty in predicting sputtering yields in fusion devices. A monolayer coverage will nearly eliminate bulk release by sputtering, and an oxide layer can reduce yields by up to a factor of ten in some cases (16).

There is considerable evidence (17,18) that sputter deposited material exhibits similar sputtering behavior as bulk material of the same composition. Redeposited plasma-side material is also expected to incorporate significant concentrations of H isotopes and He. High fluence sputtering experiments are routinely performed on projectile-saturated surfaces, and H and He loading probably alters bulk yields by less than a factor of two due to changes in S_n and particle reflection coefficients. These effects are incorporated in the existing data base.

Surface morphology can also affect sputtering yields. Roughened surfaces often show slightly higher yields than polished surfaces (9),

but with severe roughening as represented by honeycomb or matted fiber surfaces yields decrease by factors of 2-6 (19,20). The sputtering yield at glancing angles of incidence is particularly sensitive to surface morphology. The flaking of blistered surfaces can affect total erosion yields.

Although the relevance of the existing sputtering data base can be challenged on the basis of unknown surface conditions in fusion devices, it is likely that the situation is not so poorly defined. Modern cleaning techniques effectively reduce oxygen and hydrocarbon contamination and the primary effect of redeposited material is to change the mix of sputtered atoms. Erosion experiments in fusion devices (21-24) have led to results which can be understood in terms of available laboratory sputtering data. Nevertheless, surface conditions remain a major uncertainty in the sputtering of plasma-side materials.

Temperature Effects

There is no conclusive evidence that physical sputtering yields are enhanced at elevated temperatures. Light ion sputtering rates of elemental targets are unchanged at high temperature in the absence of chemical effects (25). Recent experiments using heavy ions (26) show no significant increase in the sputtering yield up to temperatures where release by evaporation exceeds sputtering by factors of three. Heavy molecular bombardment in the "spike" regime also indicates no temperature effect (27). This result does not agree with earlier experiments (28) where an increase in the sputtering yield was

observed at high temperature for heavy ions above 10 keV. No increased yields have been reported, however, for heavy ions at high temperature below 10 keV. This includes sputtering yield measurements through the melting point of low temperature metals (29). Target temperature is not a factor in the transport theory of sputtering (1). In most cases, evaporation will far exceed sputtering near the melting point.

Temperature variations related to surface and chemical effects have been reported in light and heavy ion sputtering. H sputtering of graphite increases by a factor of ~10 near 500°C due to CH_4 formation (10). He and Ar sputtering of graphite also increase with temperature (11), although the mechanism (possibly electronic) is not understood (12). The sputtering of stainless steel increases by a factor of ~2 at 400 - 500°C (30) consistent with changes in surface composition due to diffusion processes in this temperature region. The erosion yield of SiC shows up to a factor two increase at 600 - 1200°C (31,48), a temperature range where the unsputtered surface shows depletion in Si (48). Heavy ion sputtering of Ag at high fluences above 400°C increases ~30% due to cone formation (26). Temperature variations in sputtering yields not related to chemical effects or surface segregation are probably less than a factor of 2.

Multi-Component Materials

The sputtering of alloys and compounds generally leads to a depletion of the surface layers in the lighter component of the material (61). Preferential sputtering of the lighter or more easily removed component requires this depletion since the yields at large

doses must reflect bulk composition (62). The effect on total sputtering yields is small as long as the depletion does not result in the formation of a new phase with a significantly different binding energy. Fortunately, new phases are not observed (at least for sputtering at low temperature) for stainless steel and carbides which represent the most promising multi-component materials for plasma-side applications. The sputtering rates of the various components of stainless steel are similar, and data for stainless steel and Fe are almost indistinguishable (8-9). For carbides and oxides, the sputtering yield generally follows the heavy component elemental yield (5,8). Ratios of light ion sputtering yields (taken at the peak in the sputtering curve) for multi-component materials as compared with the corresponding heavy component materials are given in Table II. The multi-component yields (atoms per ion as determined by weight loss using the average atomic mass) are often slightly higher, but in many cases represent a lower net release of the heavy component than for the corresponding elemental target. Possible effects of enhanced diffusion or segregation at high temperatures in multi-component systems are probably more severe for mechanical properties than for sputtering (5).

Differential Yields

The angular and energy distributions of sputtered atoms are important in determining the transport of sputtered material in fusion devices. According to Sigmund (1), the angular distribution of sputtered atoms should be proportional to the cosine of the ejection

angle. This is generally observed for sputtering at normal incidence except for very light ions at low energy where an over-cosine distribution is found (5,32). At grazing angles of incidence, the angular distribution is peaked forward due to the increased contribution of primary recoil atoms (32,33). Computer calculations have shown this general behavior (15). The cosine distribution is probably adequate for most fusion applications.

Within the approximations of linear cascade theory (1), the flux density energy distribution for sputtered atoms in the solid angle $d\Omega$ at angle θ from the surface normal can be represented using the Thompson formula (34):

$$f(E)\, dE\, d\Omega = \frac{2 E_B}{\pi} \frac{E \cos}{(E + E_B)^3} \quad dE\, d\Omega \qquad (4)$$

where $f(E)$ is the fraction of the flux density (atoms/cm^2-s) emitted in the interval $dE\, d\Omega$ at angle θ, and E_B is the surface binding energy. This distribution has its maximum at $E_B/2$ (typically several eV) and is independent of projectile mass and energy. Experimental energy distributions generally follow Equation 4 although the maximum often differs slightly from $E_B/2$. Bay et al. (35) have observed a shift in the energy distribution to lower energies for light ions as compared to heavy ion sputtering. The maximum of the energy distribution occurs closer to $E_B/4$ for the lightest ions. This trend can be used to estimate energy distributions for various ion-target combinations; however, more measurements will be required to affect a significant improvement on Equation 4.

Conclusions

Physical sputtering data for candidate plasma-side materials in FED/INTOR are adequate for most modeling and engineering applications. Total sputtering yields are known within a factor of 2 over much of the relevant energy range for many of the ion-target combinations considered. Empirical formulations reproduce much of the available data within this accuracy. The effect of angle of incidence on the sputtering yield can be estimated from experimental results or calculated using computer codes. Target temperature does not directly influence physical sputtering yields. Multi-component materials under consideration show sputtering behavior similar to the corresponding heavy component elemental targets. Differential yields (energy and angular distributions) are in reasonable agreement with theoretical estimates and computer calculations. Surface conditions strongly influence sputtering yields and introduce major uncertainties in the application of the existing data to fusion devices. Improved understanding of surface and plasma edge conditions in fusion devices is a prerequisite for effective utilization of further refinements in the physical sputtering data base.

Acknowledgements

The author thanks M. T. Robinson and D. L. Smith for many helpful discussions during the preparation of this review.

REFERENCES

1. P. Sigmund, Phys. Rev. 184, 383 (1969), 187, 768 (1969).
2. T. J. Hoffman, H. Dodds, M. T. Robinson, and D. K. Holmes, Nucl. Sci. Eng. 68, 204 (1978); ORNL-CSD-TM-185 (1982, in press).
3. M. T. Robinson and I. M. Torrens, Phys. Rev. B9, 5008 (1974).
4. J. P. Biersack and L. G. Haggmark, Nucl. Instr. and Meth. 174, 257 (1980).
5. J. Bohdansky, J. Nucl. Mater. 93-94, 44 (1980).
6. D. L. Smith, J. N. Brooks, D. E. Post, and D. B. Heiffetz, Proc. 9th Symp. on Engineering Problems of Fusion Research, IEEE Pub. No. 81CH1715-2, p. 719 (1981).
7. W. W. Engle, Oak Ridge Gaseous Diffusion Plant report K-1693, Oak Ridge (1967). See also ref. 2.
8. J. Roth, J. Bohdansky, and W. Ottenberger, MPI für Plasmaphysik report IPP 9/26, Garching, May 1979.
9. H. H. Andersen and H. L. Bay, in Sputtering by Particle Bombardment I, edited by R. Behrisch, Springer-Verlag (1981); J. Nucl. Mater. 93-94, 625 (1980).
10. J. N. Smith and C. N. Meyer, J. Nucl. Mater. 76-77, 193 (1978).
11. J. Roth, J. Bohdansky, and K. L. Wilson, Proc. 5th Int. Conf. on Plasma Surface Interactions in Controlled Fusion Devices, Gatlinburg, TN, May 3-7, 1982.
12. V. Philipps, K. Flashkamp, and E. Vietzke, Proc. 5th Int. Conf. on Plasma Surface Interactions in Controlled Fusion Devices, Gatlinburg, TN, May 3-7, 1982.

13. L. G. Haggmark and J. P. Biersack, J. Nucl. Mater. 103-104, 345 (1981).

14. H. Oechsner, Z. Physik 261, 37 (1973).

15. L. G. Haggmark and J. P. Biersack, J. Nucl. Mater. 93-94, 664 (1980).

16. R. Behrisch, J. Roth, J. Bohdansky, A. P. Martinelli, B. Schweer, D. Rusbuldt, and E. Hintz, J. Nucl. Mater. 93-94, 645 (1980).

17. H. von Seefeld, H. Schmidl, R. Behrisch, and B. M. U. Scherzer, J. Nucl. Mater. 63, 215 (1976).

18. J. B. Roberto, R. A. Zuhr, J. L. Moore, and G. D. Alton, J. Nucl. Mater. 85-86, 1073 (1979).

19. S. N. Cramer and E. M. Oblow, Nucl. Fus. 16, 158 (1976).

20. P. J. Gierszewski, N. E. Todreas, B. Mikic, and T. F. Yang, MIT Plasma Fusion Center report PFC/RR-81-20, Cambridge, June 1981.

21. G. Staudenmaier P. Staib, G. Venus, and TFR Group, J. Nucl. Mater. 76-77, 492 (1978).

22. J. B. Roberto, R. A. Zuhr, and S. P. Withrow, J. Nucl. Mater. 93-94, 146 (1980).

23. G. Staudenmaier, J. Roth, W. R. Wampler, and ASDEX Team (unpublished).

24. R. E. Clausing, L. Heatherly, L. C. Emerson, and R. J. Colchin, Proc. 5th Int. Conf. on Plasma Surface Interactions in Controlled Fusion Devices, Gatlingurg, TN, May 3-7, 1982.

25. J. Bohdansky and J. Roth (unpublished).

26. K. Besocke, S. Berger, W. O. Hofer, and U. Littmark, Rad. Eff. (in press).

27. W. O. Hofer, K. Besocke, and B. Stritzker (unpublished).

28. R. S. Nelson, Phil. Mag. 11, 291 (1965).

29. R. C. Krutenat and C. Panzera, J. Appl. Phys. 41, 4953 (1970).

30. J. Roth, J. Bohdansky, and W. O. Hofer, p. 309 in Proc. Int. Symp. on Plasma Wall Interaction, Jülich 1976 (Pergammon Press, Oxford, 1977).

31. J. Roth, J. Bohdansky, W. Poschenreider, and M. K. Sinha, J. Nucl. Mater. 63, 222 (1976).

32. H. L. Bay, J. Bohdansky, W. O. Hofer, and J. Roth, Appl. Phys. (in press).

33. B. M. Gurmin, Yu. A. Ryzhov, and I. I. Shkrarban, Bull. Akad. Sci. USSR Physics Ser. (USA) 33, 752 (1968).

34. M. W. Thompson, Phil. Mag. 18, 377 (1968).

35. H. L. Bay, W. Berres, and E. Hintz, Nucl. Instrum. and Meth. 194, 555 (1982).

36. J. Roth, J. Bohdansky, R. S. Blewer, W. Ottenberger, and J. Borders, J. Nucl. Mater. 85-86, 1077 (1979).

37. J. A. Borders, R. A. Langley, and K. L. Wilson, J. Nucl. Mater. 76, 168 (1978).

38. H. Fetz and H. Oechsner, p. 39 in Proc. 6th Int. Conf. Phenomenes d'Ionisations das les Gaz, Paris (1963).

39. N. Laegreid and G. K. Wehner, J. Appl. Phys. 32, 365 (1961).

40. J. Roth, J. Bohdansky, P. A. Martinelli, Proc. Int. Conf. on Ion Beam Modification of Materials, Budapest (Sept. 1981).

41. S. Miyagawa, Y. Ato, and Y. Morita, J. Appl. Phys. 49, 6164 (1978).

42. J. N. Smith, C. H. Meyer, and J. K. Layton, J. Nucl. Mater. 67, 234 (1977).

43. D. Rosenberg and G. K. Wehner, J. Appl. Phys. 33, 1842 (1962).

44. G. K. Wehner, General Mills Report No. 2309 (1962).

45. E. Hechtl, J. Bohdansky, and J. Roth, J. Nucl. Mater. 103-104, 333 (1981).

46. O. Almen and G. Bruce, Nucl. Instrum. Methods 11, 257 and 279 (1961).

47. K. Sone, M. Saidoh, K. Nakamura, R. Yamada, Y. Murakami, T. Skikama, M. Fukutomi, M. Kitajima, and M. Okada, J. Nucl. Mater. 98, 270 (1981).

48. M. Mohri, K. Watanabe, T. Yamashina, H. Doi, and K. Hayakawa, J. Nucl. Mater. 85-86, 1185 (1979).

49. J. Bohdansky, H. L. Bay, and W. Ottenberger, J. Nucl. Mater. 76-77, 163 (1978).

50. A. Southern, W. R. Willis, and M. T. Robinson, J. Appl. Phys. 34, 153 (1963).

51. O. V. Kurbatov, Sov. Phys. - Tech. Phys. 12, 1328 (1968).

52. M. Kaminsky, J. Vac. Sci. Tech. 20, 1304 (1982).

53. W. O. Hofer, H. L. Bay, and P. J. Martin, J. Nucl. Mater. 76, 156 (1978).

54. H. L. Bay, W. O. Hofer, and J. Bohdansky (unpublished).

55. J. Bohdansky, H. L. Bay, and J. Roth, p. 1509 in Proc. 7th Int. Vacuum Congress and 3rd Int. Conf. on Solid Surfaces, Vienna (1977).

56. C. H. Weijsenfeld, A. Haagendoorn, and M. Koedam, Physica 27, 763 (1961).

57. H. L. Bay, J. Roth, and J. Bohdansky, J. Appl. Phys. 48, 4722 (1977).

58. H. Ohtsuka, R. Yamada, K. Sone, M. Saidoh, and T. Abe, J. Nucl. Mater. 76, 188 (1978).

59. C. R. Finfgeld, Oak Ridge Operations report ORO-3557-15, Oak Ridge (1970).

60. G. K. Wehner, Phys. Rev. 108, 35 (1957).

61. E. Taglauer and W. Heiland, Proc. Symp. on Sputtering, Perchtoldsdorf/Vienna (1980).

62. H. H. Andersen, in SPIG 1980, ed. by B. Cobic, Boris Kidric Institute of Nuclear Sciences, Belgrade (1980).

Table I. Normal incidence yields for D and selfion sputtering of candidate materials at 0.3, 1, and 3 keV. Self-sputtering exceeds unity for V (≳800 eV), stainless steel (>500 eV), Mo (>700 eV) and W (>600 eV). Estimated accuracies are ±50% for D sputtering and within a factor of two for self-sputtering.

Material	D Sputtering Yield (atoms/D)			Self-Sputtering Yield (atoms/ion)		
	300 eV	1 keV	3 keV	300 eV	1 keV	3 keV
Be	0.02	0.03	0.02	0.5	0.6	0.5
B	0.03	0.03	0.02	~0.4	~0.6	~0.5
C	0.03	0.02	0.01	0.3	0.5	0.5
SiC	0.02	0.03	0.02	0.3	0.6	0.8
TiC	0.01	0.02	0.02	0.3	0.5	0.9
V	~0.01	~0.03	~0.03	~0.3	~1	>1
stainless steel	0.01	0.03	0.02	0.6	1.4	1.6
Mo	0.002	0.007	0.008	0.5	1.3	2
W	2×10^{-4}	0.002	0.005	0.4	1.3	2

Table II. Relative peak sputtering yields for light ions incident on multi-component materials and the corresponding heavy component elemental targets. The ratios are compiled from ref. 8.

Multi-Component Target	Elemental Target	Yield Ratio (Multi-Component/Elemental)
Al_2O_3	Al	1.2
Inconel	Ni	~1
SiC	Si	1.2
SiO_2	Si	1.5
Stainless steel	Fe	~1
TaC	Ta	1.6
Ta_2O_5	Ta	3
TiC	Ti	1.6
WC	W	3

FIGURE CAPTIONS

Fig. 1. Comparison of experimental normal incidence sputtering yields (5) for Mo targets with calculated yields from the IPP model (5) and DSPUT (6).

Fig. 2. Normal incidence sputtering yields for Be targets (refs. 36-39). These data are similar to results obtained for a BeO target and may be representative of the oxide surface.

Fig. 3. Normal incidence sputtering yields for B (and B_4C) targets (refs. 40-41).

Fig. 4. Normal incidence sputtering yields for C and graphite targets (refs. 40, 37, 42-46).

Fig. 5. Normal incidence sputtering yields for SiC (and Si) targets (refs. 39, 45, 47-50). Calculated yields for Si and C on SiC are also shown.

Fig. 6. Normal incidence sputtering yields for TiC (and Ti) targets (refs. 45, 46, 39, 49, 51, 52). Calculated yields for Ti and C on TiC are also shown.

Fig. 7. Normal incidence sputtering yields for V targets (refs. 43, 46, 39, 53, 54).

Fig. 8. Normal incidence sputtering yields for stainless steel targets (refs. 17, 18, 50, 39, 55, 56).

Fig. 9. Normal incidence sputtering yields for Mo targets (refs. 43, 46, 9, 57-59).

Fig. 10. Normal incidence sputtering yields for W targets (refs. 40, 45, 46, 60).

Fig. 11. Variation of the sputtering yield with angle of incidence (refs. 14, 8). Calculated results using TRIM (13), ANISN (2), and DSPUT (6) are also shown. Solid curves are to guide the eye.

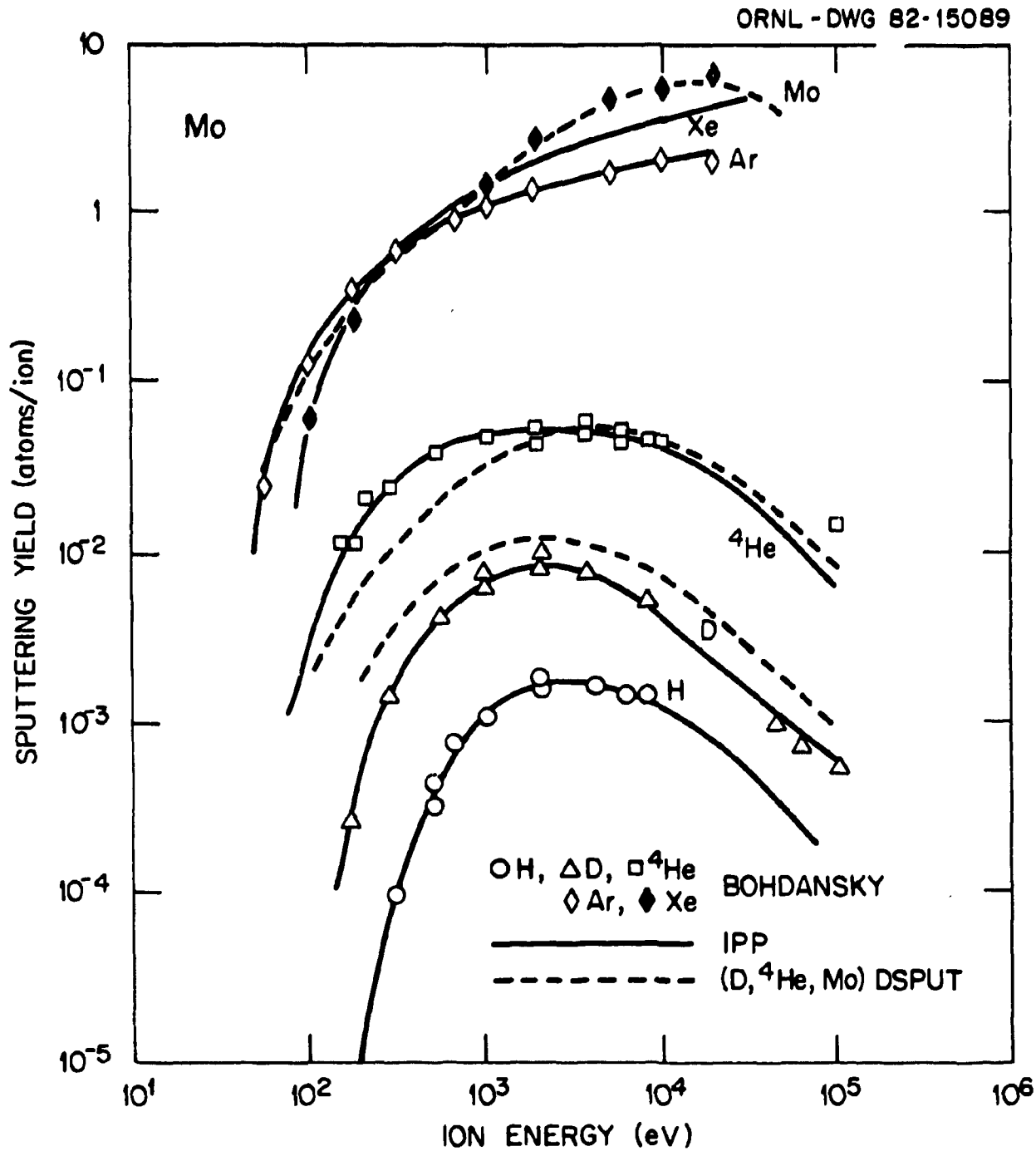
ORNL - DWG 82-15089
Mo
Mo
Xe
Ar
^{4}He
D
H
SPUTTERING YIELD (atoms/ion)
ION ENERGY (eV)
10
1
10^{-1}
10^{-2}
10^{-3}
10^{-4}
10^{-5}
10^1
10^2
10^3
10^4
10^5
10^6
O H, △ D, □ ^{4}He
◊ Ar, ♦ Xe
BOHDANSKY
IPP
(D, ^{4}He, Mo) DSPUT

FIG. 1

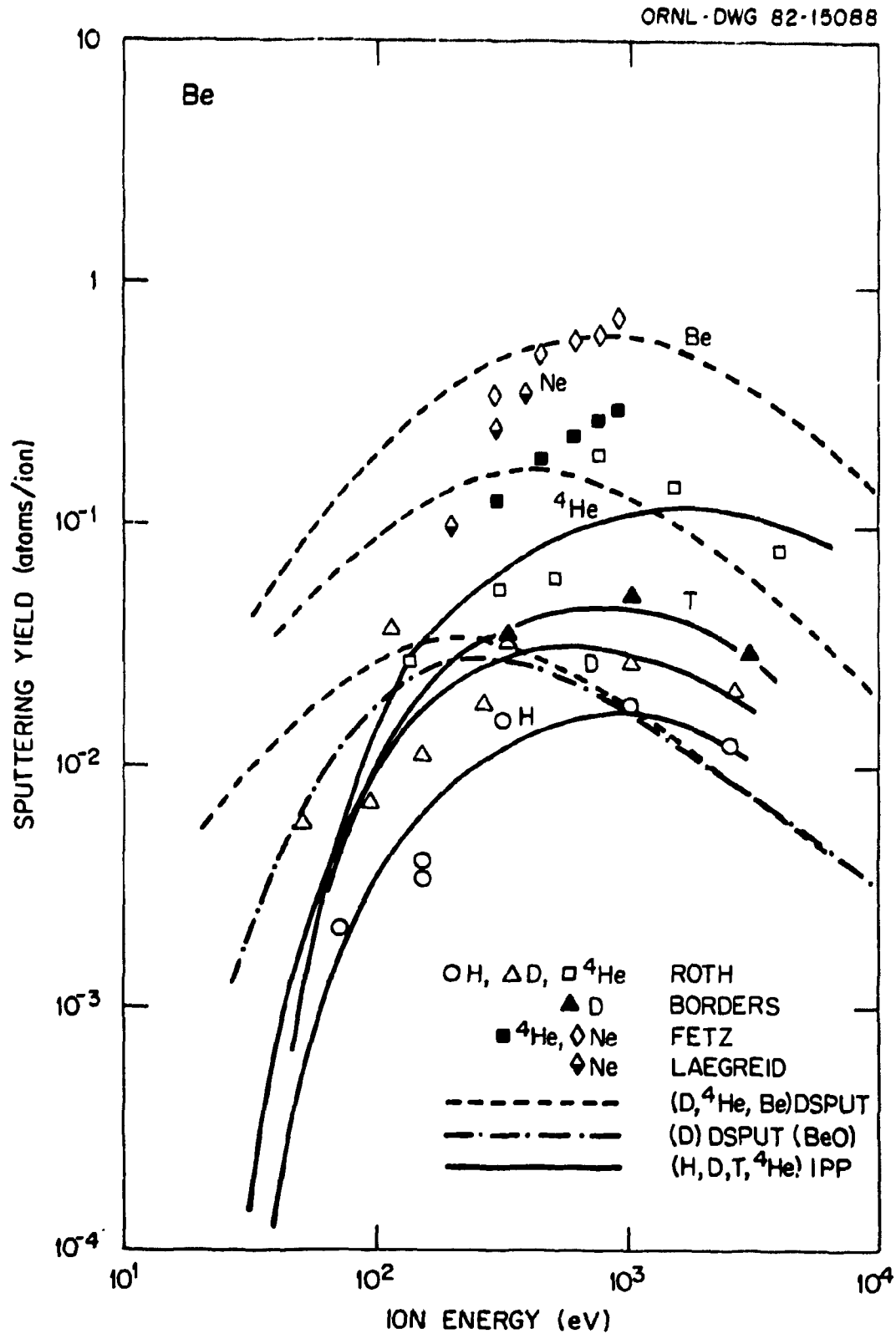
ORNL-DWG 82-15088
Be
SPUTTERING YIELD (atoms/ion)
ION ENERGY (eV)
10
1
10^{-1}
10^{-2}
10^{-3}
10^{-4}
10^{1}
10^{2}
10^{3}
10^{4}
Be
Ne
^{4}He
T
D
H
O H, Δ D, □ ^{4}He ROTH
▲ D BORDERS
■ ^{4}He, ◊ Ne FETZ
◆ Ne LAEGREID
(D, ^{4}He, Be) DSPUT
(D) DSPUT (BeO)
(H, D, T, ^{4}He) IPP

FIG. 2

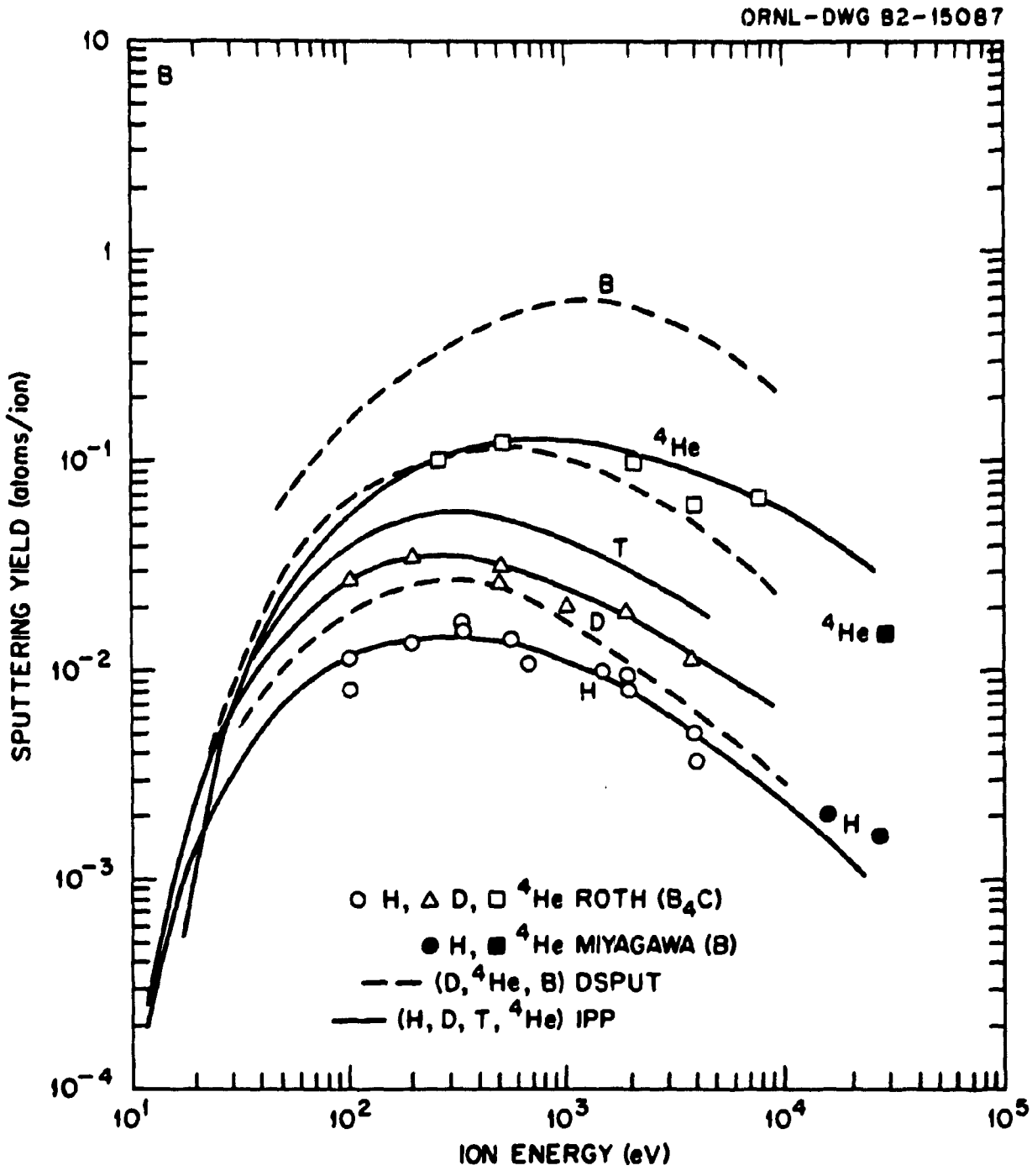
ORNL-DWG 82-15087
SPUTTERING YIELD (atoms/ion)
ION ENERGY (eV)
B
4He
T
D
H
○ H, △ D, □ 4He ROTH (B4C)
● H, ■ 4He MIYAGAWA (B)
(D, 4He, B) DSPUT
(H, D, T, 4He) IPP

FIG. 3

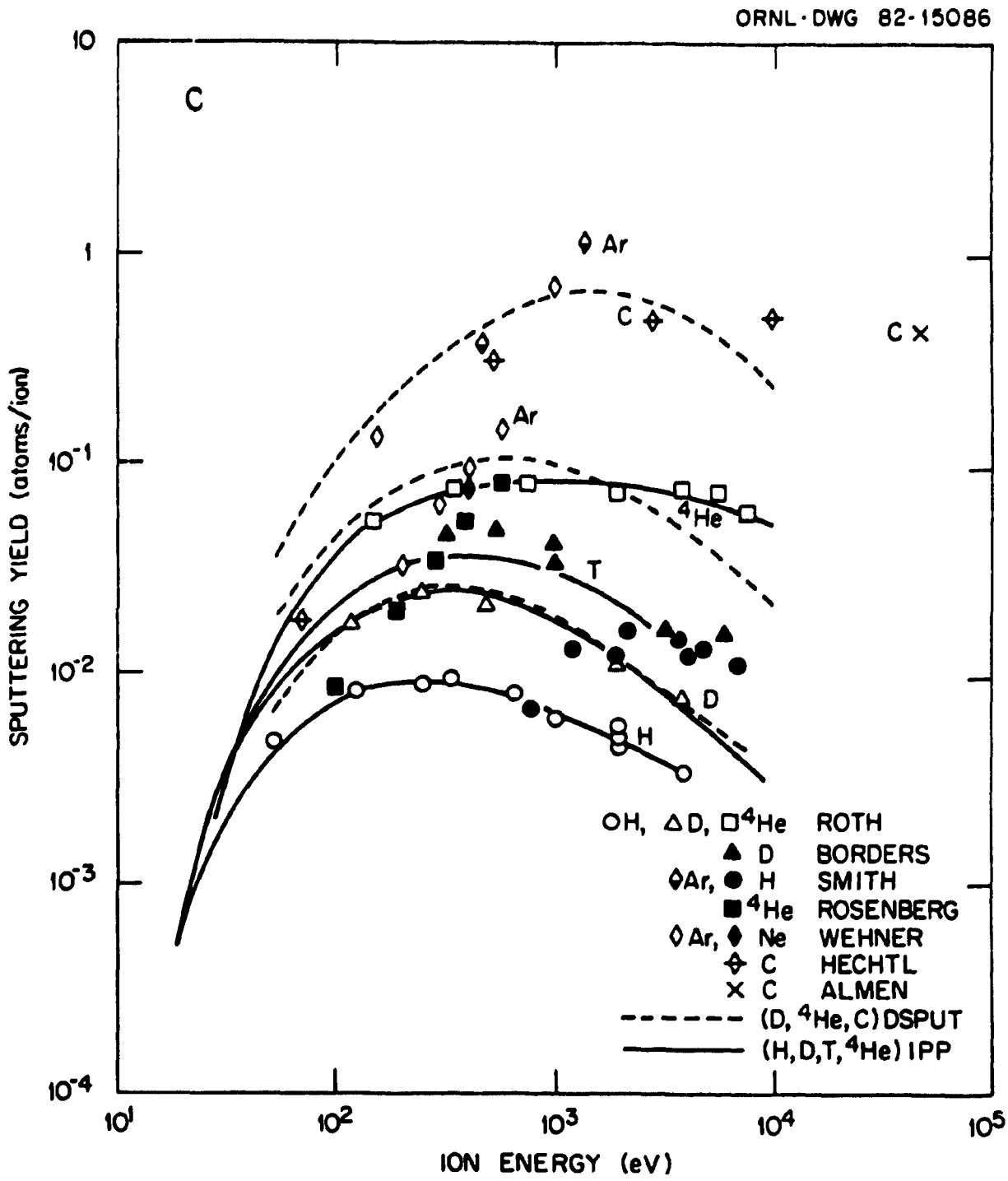
ORNL-DWG 82-15086
C
Ar
C
C x
Ar
4He
T
D
H
OH, △D, □4He ROTH
▲ D BORDERS
◊Ar, ● H SMITH
■4He ROSENBERG
◊Ar, ♦ Ne WEHNER
◇ C HECHTL
× C ALMEN
(D, 4He, C) DSPUT
(H, D, T, 4He) IPP
SPUTTERING YIELD (atoms/ion)
ION ENERGY (eV)
10
1
10-1
10-2
10-3
10-4
101
102
103
104
105

FIG. 4

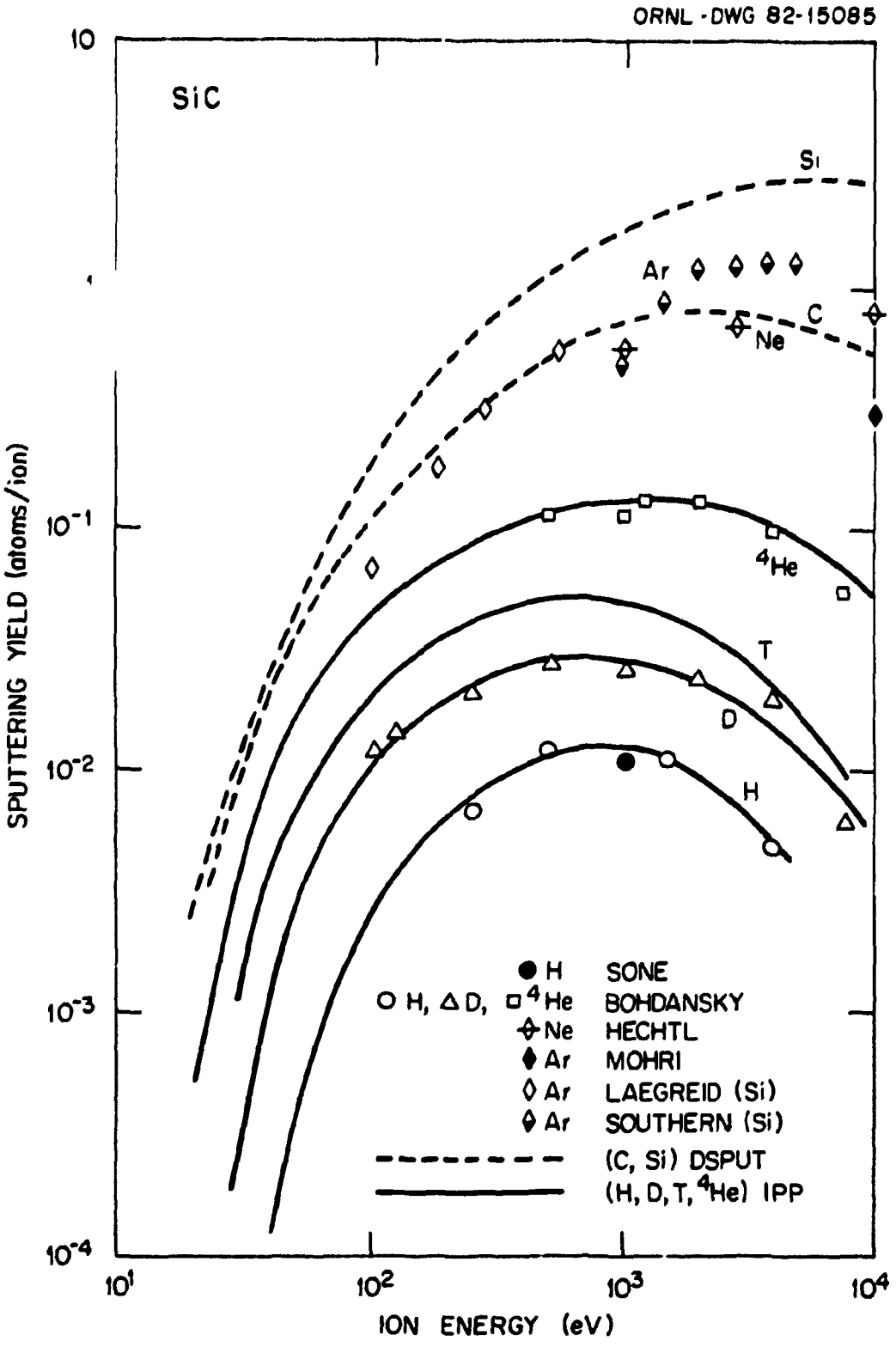
ORNL-DWG 82-15085
SiC
Si
Ar
C
Ne
^{4}He
T
D
H
SPUTTERING YIELD (atoms/ion)
ION ENERGY (eV)
10
10^{-1}
10^{-2}
10^{-3}
10^{-4}
10^1
10^2
10^3
10^4
● H SONE
○ H, △ D, □ ^{4}He BOHDANSKY
⊕ Ne HECHTL
♦ Ar MOHRI
◊ Ar LAEGREID (Si)
♦ Ar SOUTHERN (Si)
(C, Si) DSPUT
(H, D, T, ^{4}He) IPP

FIG. 5

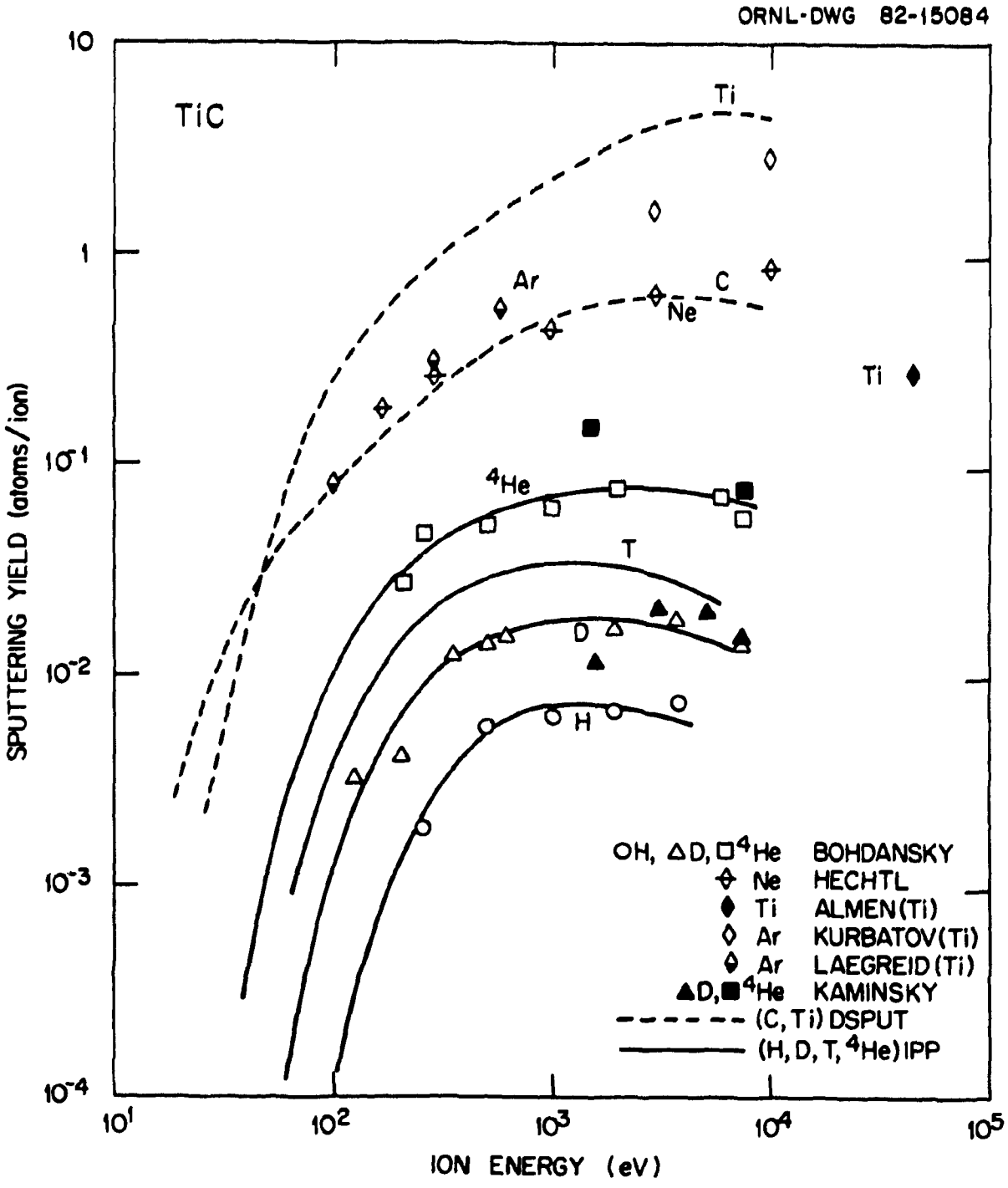
ORNL-DWG 82-15084
TiC
Ti
Ar
C
Ne
Ti
^{4}He
T
D
H
SPUTTERING YIELD (atoms/ion)
ION ENERGY (eV)
10
1
10^{-1}
10^{-2}
10^{-3}
10^{-4}
10^1
10^2
10^3
10^4
10^5
○H, △D, □^{4}He BOHDANSKY
◇ Ne HECHTL
♦ Ti ALMEN(Ti)
◊ Ar KURBATOV(Ti)
♦ Ar LAEGREID(Ti)
▲D, ■^{4}He KAMINSKY
(C, Ti) DSPUT
(H, D, T, ^{4}He) IPP

FIG. 6

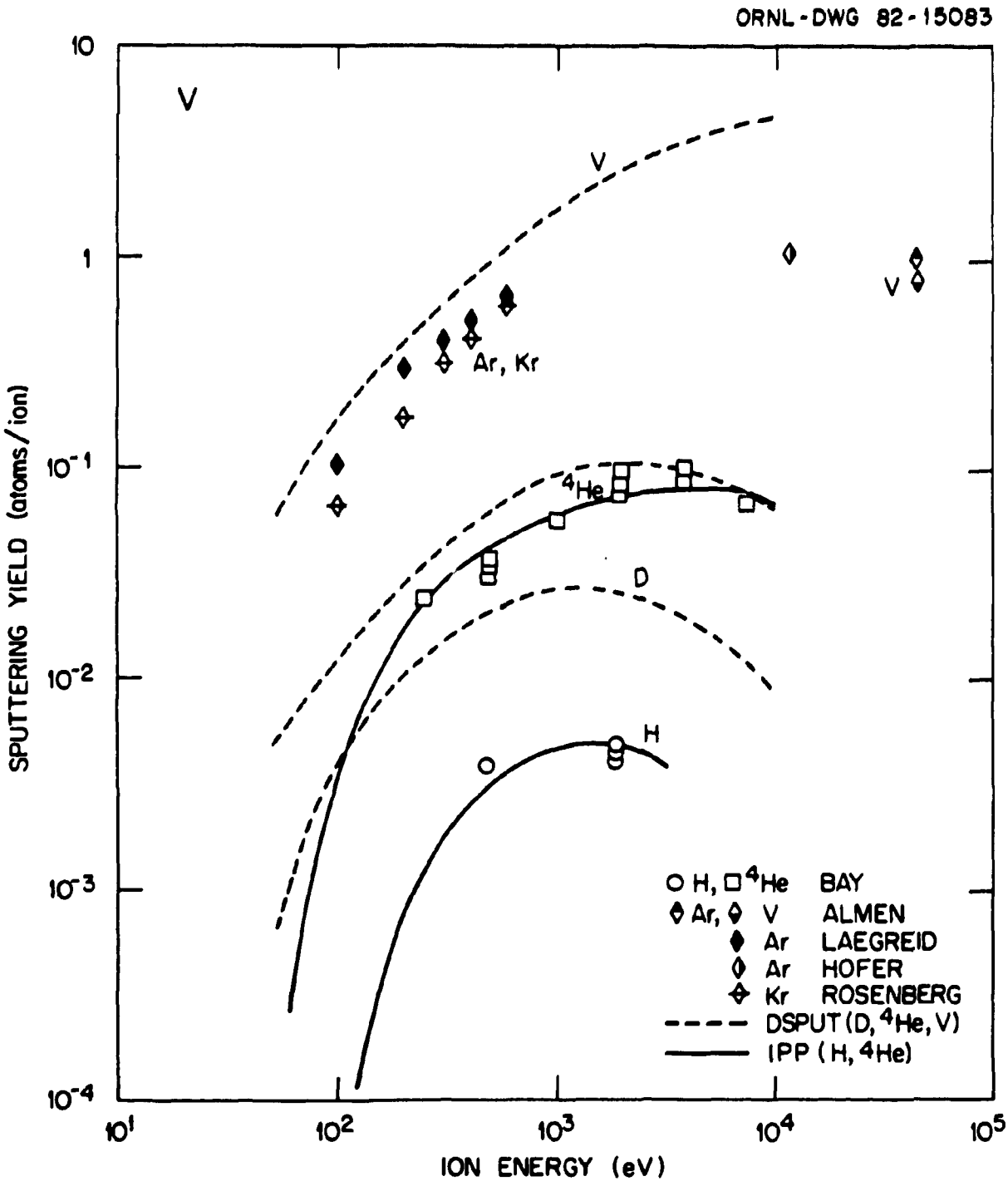
ORNL-DWG 82-15083
V
V
V
V
Ar, Kr
^{4}He
D
H
O
SPUTTERING YIELD (atoms/ion)
ION ENERGY (eV)
10
1
10^{-1}
10^{-2}
10^{-3}
10^{-4}
10^1
10^2
10^3
10^4
10^5
O H, □ ^{4}He BAY
◊ Ar, ◊ V ALMEN
◆ Ar LAEGREID
◊ Ar HOFER
◈ Kr ROSENBERG
DSPUT (D, ^{4}He, V)
IPP (H, ^{4}He)

FIG. 7

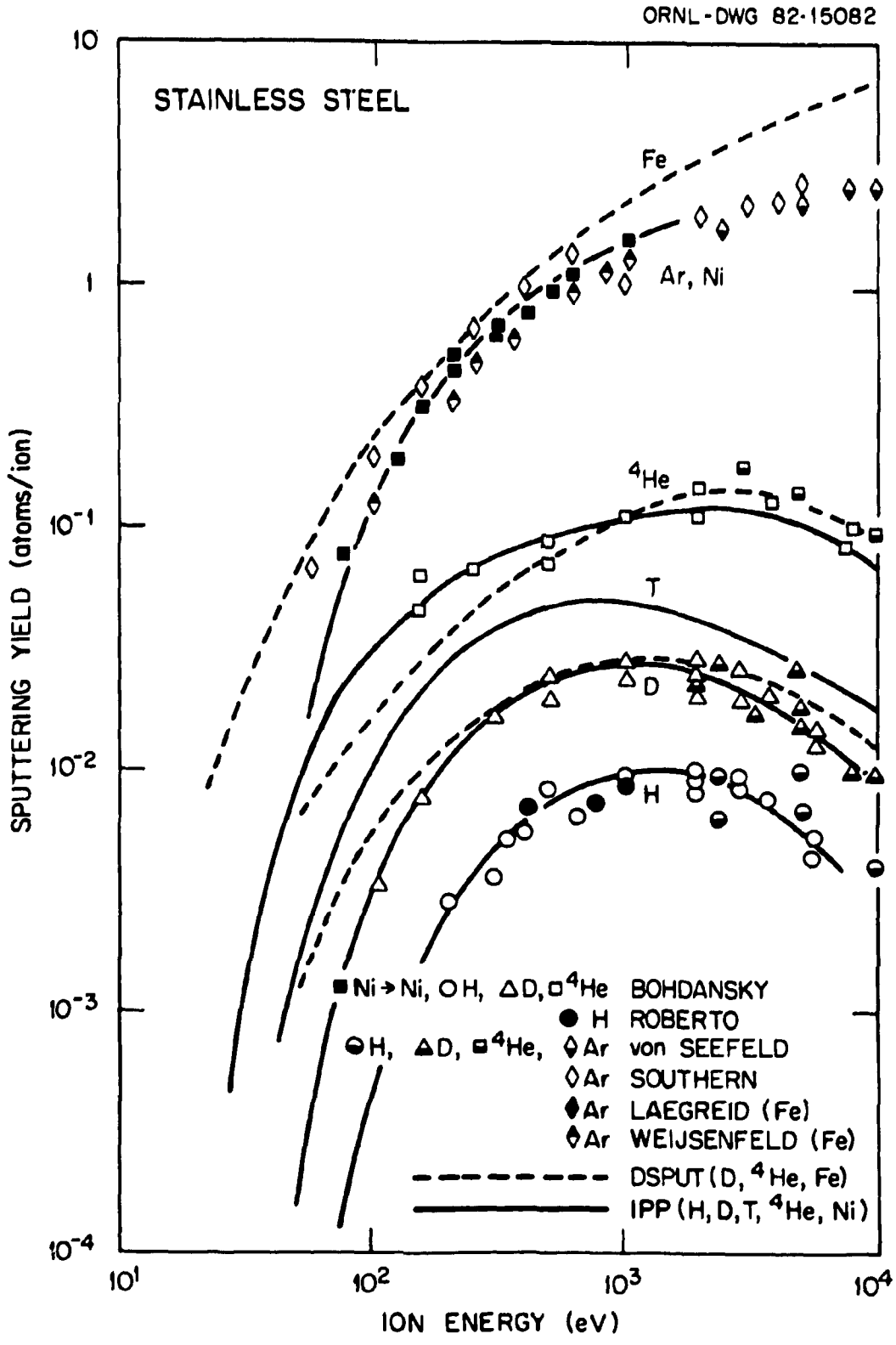
ORNL-DWG 82-15082
STAINLESS STEEL
Fe
Ar, Ni
^{4}He
T
D
H
SPUTTERING YIELD (atoms/ion)
ION ENERGY (eV)
10
1
10^{-1}
10^{-2}
10^{-3}
10^{-4}
10^1
10^2
10^3
10^4
■ Ni → Ni, ○ H, △ D, □ ^{4}He BOHDANSKY
● H ROBERTO
⊖ H, ▲ D, ▪ ^{4}He, ◊ Ar von SEEFELD
◊ Ar SOUTHERN
◆ Ar LAEGREID (Fe)
◊ Ar WEIJSENFELD (Fe)
DSPUT (D, ^{4}He, Fe)
IPP (H, D, T, ^{4}He, Ni)

FIG. 8

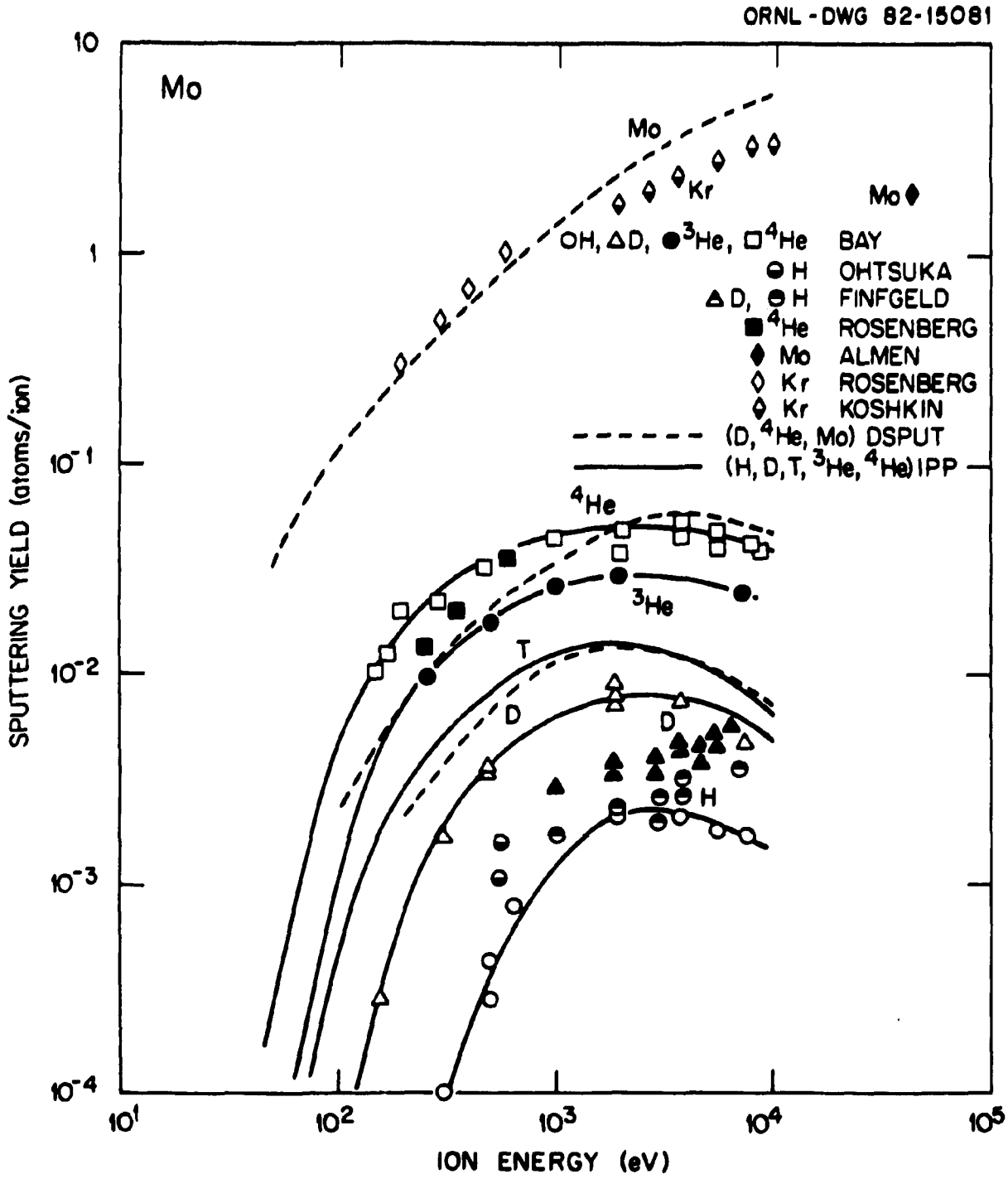
ORNL-DWG 82-15081
Mo
Mo
Kr
Mo
OH, D, ^{3}He, ^{4}He BAY
H OHTSUKA
D, H FINFGELD
^{4}He ROSENBERG
Mo ALMEN
Kr ROSENBERG
Kr KOSHKIN
(D, ^{4}He, Mo) DSPUT
(H, D, T, ^{3}He, ^{4}He) IPP
^{4}He
^{3}He
T
D
D
H
SPUTTERING YIELD (atoms/ion)
ION ENERGY (eV)
10
1
10^{-1}
10^{-2}
10^{-3}
10^{-4}
10^1
10^2
10^3
10^4
10^5

FIG. 9

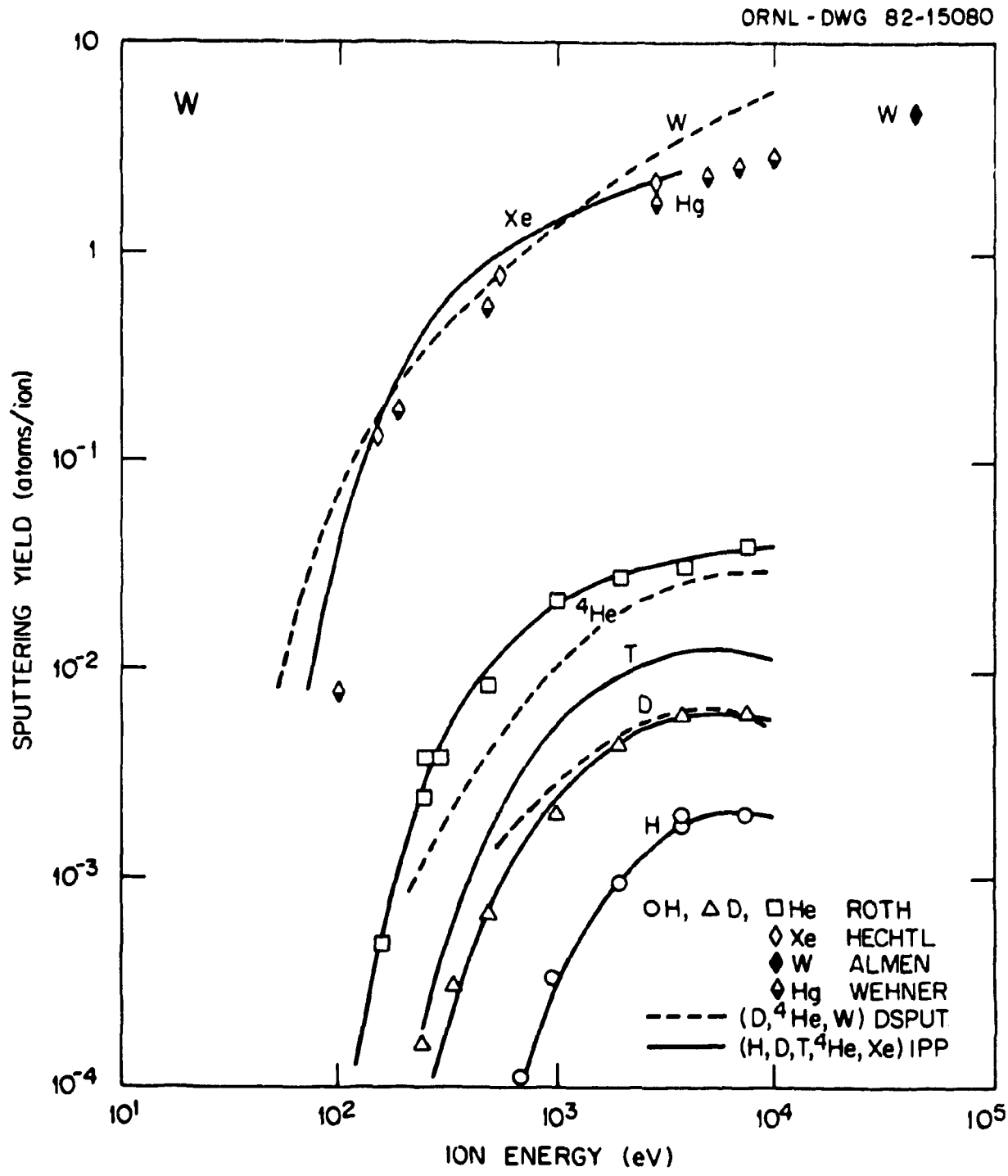
ORNL - DWG 82-15080
W
W
W
Xe
Hg
^{4}He
T
D
H
SPUTTERING YIELD (atoms/ion)
ION ENERGY (eV)
10
1
10^{-1}
10^{-2}
10^{-3}
10^{-4}
10^1
10^2
10^3
10^4
10^5
OH, △D, □He ROTH
◊Xe HECHTL
♦W ALMEN
◊Hg WEHNER
(D,^{4}He,W) DSPUT
(H,D,T,^{4}He,Xe) IPP

FIG. 10

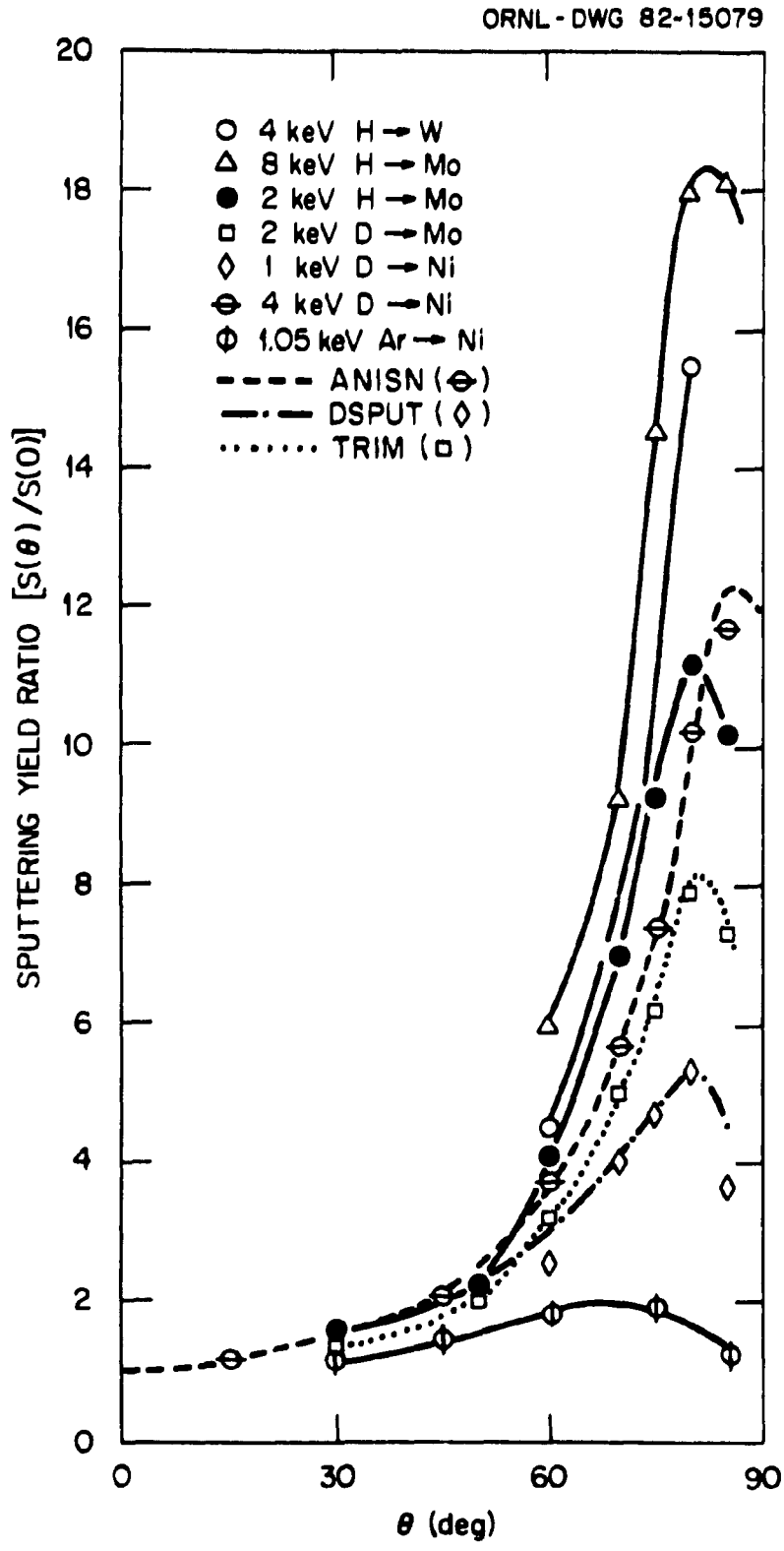
ORNL - DWG 82-15079
SPUTTERING YIELD RATIO [S(θ)/S(0)]
θ (deg)
0
2
4
6
8
10
12
14
16
18
20
0
30
60
90
4 keV H → W
8 keV H → Mo
2 keV H → Mo
2 keV D → Mo
1 keV D → Ni
4 keV D → Ni
1.05 keV Ar → Ni
ANISN (⊖)
DSPUT (◊)
TRIM (□)

FIG. 11